Broadband Terahertz Generation and Detection at 10 Nanometer Scale.

ARTICLE *in* NANO LETTERS · MAY 2013

Impact Factor: 13.59 · DOI: 10.1021/nl401219v · Source: PubMed

NANO LETTERS

Letter

pubs.acs.org/NanoLett

Broadband Terahertz Generation and Detection at 10 nm Scale

Yanjun Ma,[†] Mengchen Huang,[†] Sangwoo Ryu,[‡] Chung Wung Bark,[‡,§] Chang-Beom Eom,[‡] Patrick Irvin,[†] and Jeremy Levy*[,†]

[†]Department of Physics and Astronomy, University of Pittsburgh, Pittsburgh, Pennsylvania 15260, United States

[‡]Department of Materials Science and Engineering, University of Wisconsin-Madison, Madison, Wisconsin 53706, United States

Supporting Information

ABSTRACT: Terahertz (0.1−30 THz) radiation reveals a wealth of information that is relevant for material, biological, and medical sciences with applications that span chemical sensing, high-speed electronics, and coherent control of semiconductor quantum bits. To date, there have been no methods capable of controlling terahertz (THz) radiation at molecular scales. Here we report both generation and detection of broadband terahertz field from 10 nm scale oxide nanojunctions. Frequency components of ultrafast optical radiation are mixed at these nanojunctions, producing broadband THz emission. These same devices detect THz electric fields with comparable spatial resolution. This unprecedented control, on a scale of 4 orders of magnitude smaller than the diffraction limit, creates a pathway toward THz-bandwidth spectroscopy and control of individual nanoparticles and molecules.

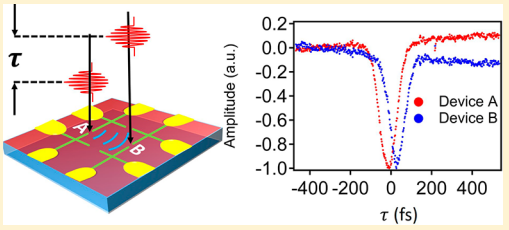

KEYWORDS: *Optical rectification, THz field, nanoscale photoconductivity, oxide nanostructure*

The spatial resolution and spectral range of optical probes has advanced considerably in the last two decades. Near-field optical techniques[1−3] have been used to characterize single molecules[4] and semiconductor nanostructures,[5] offering insights into properties that are inaccessible from measurements on ensembles.

The terahertz (THz) portion of the electromagnetic spectrum couples to a range of excitations in molecules,[6,7] solid-state qubits,[8] and devices.[9] For THz spectroscopy and control to achieve the resolution level of a single molecule, diverse approaches have been explored. Nanoscale THz sources[10] and submicrometer detectors[11] have been experimentally realized. Terahertz near-field imaging can achieve subwavelength spatial resolution with metallized tips[9,12] and near-field detectors.[13,14] However, to date the technology for THz imaging and spectroscopy has not reached a spatial resolution or sensitivity necessary for single-molecule studies.

Here we describe the creation of a new class of nanoscale THz sources and detectors formed at the $LaAlO_3/SrTiO_3$ (LAO/STO) interface (Figure 1A,B).[15] When the LAO layer is at or close to a critical thickness of 3 unit cells (u.c.), the metal−insulator transition can be locally and reversibly controlled using a conductive atomic force microscope (c-AFM) tip.[16] A variety of nanoscale electronic[17−19] and photonic[20] devices have already been demonstrated.

$SrTiO_3$ has one of the largest known third-order nonlinear optical susceptibilities in the solid state.[21] In the experiments described here, the optical fields $E^i_{opt}(\omega)$ are localized in time (~30 fs duration), and confined to ~1 μm in the plane of the junction (see the Supporting Information for details.). The quasistatic field from the source bias E^i_{bias} is localized within a volume $V \sim 10$ nm^3, defined by the spatial extent of the nanowire that is known from prior investigations.[20,22] Owing to the nonlinear process occurring in the nanojunction area, the resulting polarization P^i_{NL} can combine the spatial resolution of the bias field and temporal resolution of the optical field (Figure 1C) (see the Supporting Information for details.). Motivated by the fact that THz fields can be produced and sensed via $\chi^{(3)}$ processes,[23,24] LAO/STO can be an attractive potential platform for optically generating and detecting THz at scales close to a single particle.

Figure 2A illustrates the basic experimental setup to demonstrate the feasibility of generating THz field at nanoscale. A nanojunction, consisting of a ~10 nm wide nanowire with a ~10 nm insulating barrier, is fabricated at the LAO/STO interface with c-AFM lithography (see the Supporting Information for details). Ultrafast (~30 fs) optical pulses from a Ti:Sapphire laser are divided into "pump" and "probe" beams by a Mach−Zehnder interferometer. Photoconductive properties are measured using a four-terminal geometry in which a voltage is applied between source (S) and drain (D) electrodes, and two voltage sensing electrodes, V_+ and V_-, are used to measure the photoinduced differential voltage $\Delta V_{ph} = V_+ - V_-$. All experiments are performed at 80 K except where noted.

By measuring ΔV_{ph} as a function of the (x,y) coordinate of the focused light spot,[20,25] a photoconductive image is generated. In Figure 2B, the diffraction-limited peak shows where the nanojunction was created. By allowing both beams to illuminate the nanojunction and scanning the optical delay line

Received: April 4, 2013
Revised: May 10, 2013
Published: May 21, 2013

   dx.doi.org/10.1021/nl401219v | *Nano Lett.* 2013, 13, 2884−2888

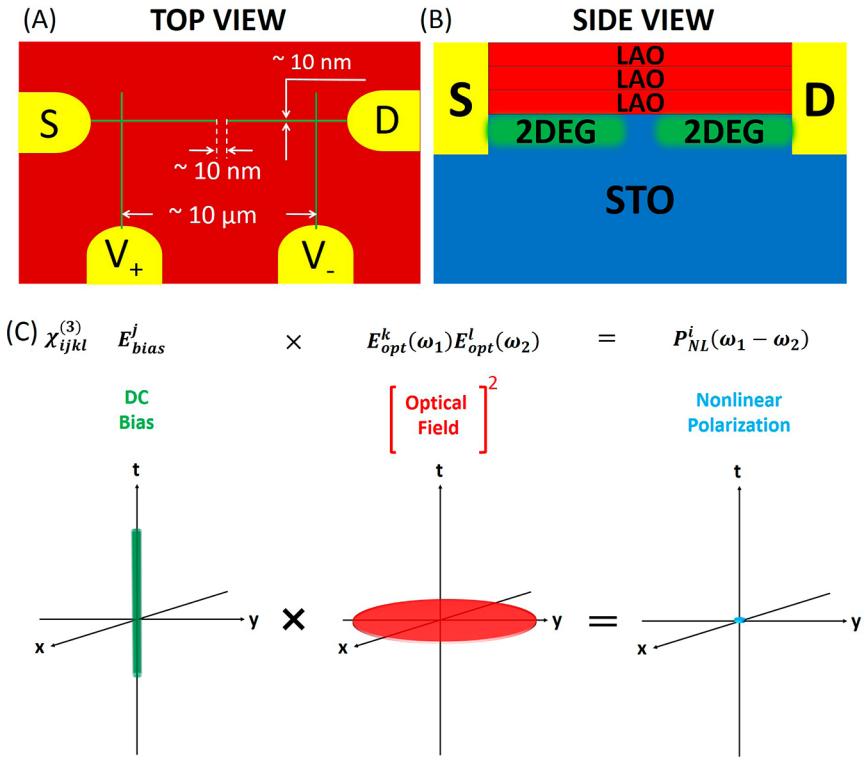

Figure 1. Device structure and the spatiotemporal confinement of the nonlinear polarization. (A) The top view shows the typical device geometry used in our experiments. (B) Cross-sectional view shows the formation of 2DEG at the interface of $LaAlO_3$ and $SrTiO_3$ due to the potential on a c-AFM tip. (C) The DC bias field is local in space, while the optical field is local in time. Consequently, the $\chi^{(3)}$ polarization is confined both spatially and temporally.

(ODL), dynamical information can be resolved. In Figure 2C, when the chopper is off, interference fringes are observed that are attributed to field autocorrelation. It is noticed that the lower envelope shows larger amplitude than the upper one. By turning the chopper on, lock-in detection can filter away the fast oscillations, leaving only the asymmetric envelope to be detected by averaging over a large number of measurements. The response exhibits a full width at half-maximum (fwhm) of 31 fs (Figure 2D).

The spatial and temporal response of the device can be measured by repeating the time-resolved measurement at a regular two-dimensional array of locations. The result shows that the temporal dynamics is highly localized around the junction area and can be tuned by the dc bias across the junction (see Supporting Information Figures S3 and S4), which agrees with the picture shown in Figure 1C. Experiments characterizing the nonlinear properties of the nanojunction are detailed in the Supporting Information.

To illustrate that the THz field can be generated and detected by the nanojunction, an experiment is performed with two identical nanojunctions, separated by a distance Δx (Figure 3A). Each nanostructure is illuminated with a focused optical spot.

The detection occurs when the THz field E_{THz} produced at one junction (source) interacts with the optical field E_{opt} around the other junction (detector). The resulting polarization via the $\chi^{(3)}$ process $P_{NL} \propto E_{THz}E^2_{opt}$ acts on the detector as a field offsetting the nanoscale photoconductivity. The temporal resolution is provided by the laser pulse, as indicated by $P_{NL} \propto E_{THz}E^2_{opt}$. The spatial resolution is again determined by the gap. Although the double-junction experiment does not directly demonstrate the spatial resolution for THz near-field imaging, based on the above analysis and physical mechanism, it is a reasonable conclusion that the scale of the nanojunction determines the resolution in the near-field region. This field sensing mechanism is analogous to work described in refs 14 and 26; however, our detection mechanism is fundamentally different in that the field confinement required by near-field measurement is provided by the spatial confinement of E_{bias} around the nanojunction.[20] The results discussed here are for $\Delta x = 12$ μm; similar measurements with $\Delta x = 6$ μm are shown in the Supporting Information.

The locations of the two junctions are confirmed by overlapping the ΔV_{ph} image with a simultaneously acquired confocal reflectivity image. In Figure 3B,C, the surrounding electrodes are imaged via the sample reflectance; the red spot corresponds to the ΔV_{ph} image, indicating the location of the nanojunction. The two junctions are electrically isolated from one another, as confirmed by $I-V$ measurements (Supporting Information Figure S9).

Both beams are intensity modulated but at different frequencies: the pump beam, focused on Junction A (the device measured in Figure 3B), is modulated at frequency $f_A \approx$ 380 Hz while the probe beam, focused on Junction B (the device measured in Figure 3C), is modulated at frequency $f_A \approx$ 460 Hz. During the scan of optical delay line, the ΔV_{ph} in Junction A is detected by a lock-in amplifier at frequency f_B. Similarly, the ΔV_{ph} in Junction B is measured by a second lock-in amplifier at frequency f_A. In this configuration, the THz field generated by one nanojunction can simultaneously be probed by the other. The ODL is stepped and the piezo shaker used for the single junction characterizations (see the Methods in Supporting Information) is turned off for this experiment, making it sensitive to any optical interference effects. A time

dx.doi.org/10.1021/nl401219v | Nano Lett. 2013, 13, 2884−2888

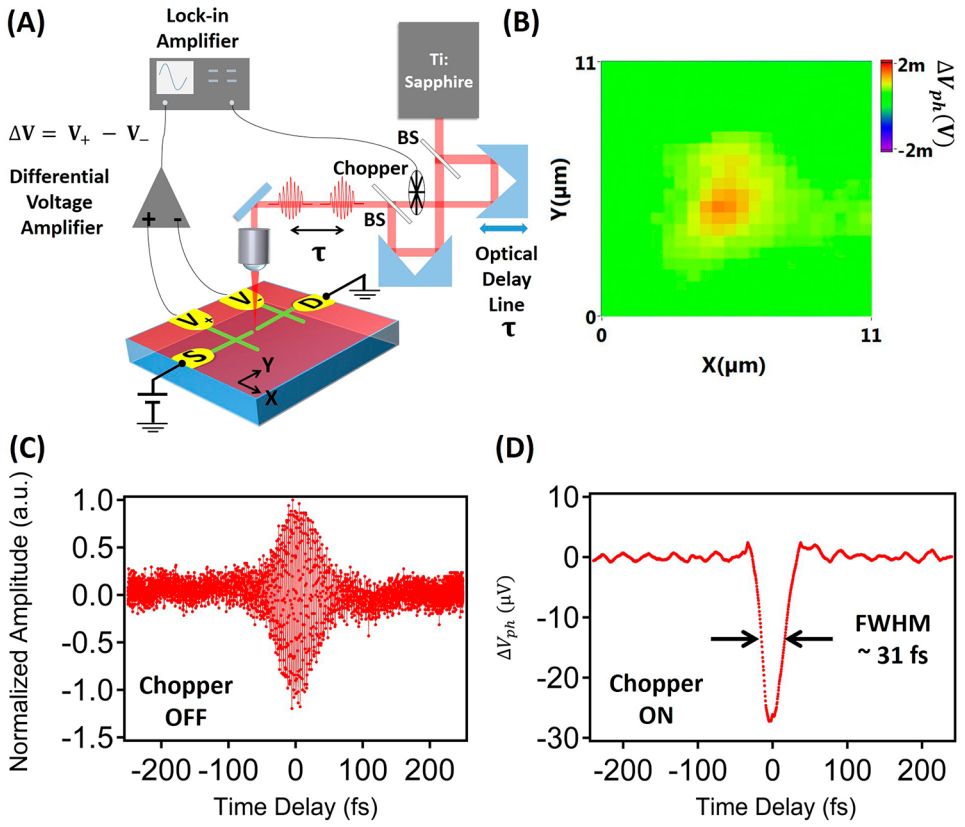

Figure 2. Time-resolved photoresponse measurement. (A) Representation of the experimental setup. X and Y indicate the scanning axes. BS: ultrafast beam splitter. (B) ΔV_{ph} image with the color scale showing its amplitude. ($I_{ave} \approx 10$ kW/cm^2 and $V_s = -1$ V.) (C) Time-resolved measurement. Interference fringes are observed when the chopper is turned off. (D) Time-resolved measurement with the chopper on. Offsets have been subtracted. This is the average over 120 measurements. ($I_{ave} \approx 50$ kW/cm^2 for both pulses and $V_s = -1$ V.).

delay of approximately $\Delta\tau \approx 44$ fs between the two peaks is found in Figure 3D. Typical voltages measured in these time-resolved experiments are on the order of 10−100 μV.

The spot size of both pump and probe light has been carefully measured to make sure that there is no overlap between them (see the Supporting Information). Because the ΔV_{ph} at Junction B is being measured at frequency f_A (and vice versa), the detected signal must result from an interaction between the local field and an electric field $E_{emit}(t)$, generated by the other remote junction. The field $E_{emit}(t)$ cannot be an optical field; otherwise one would observe interference fringes as shown in Figure 2C; such interference is not observed (Figure 3D). A Fourier transform (Figure 3E) reveals a spectral peak at 1 THz with a 3 dB-bandwidth around 3 THz and spectral content extending to 10 THz, which indicates that $E_{emit}(t)$ should be the THz emission from one junction that is detected at the other one. Here the frequency resolution is limited by the delay scan length (1 ps^{-1} = 1 THz). Also, the spatial extent of the THz emission and detection is not determined by the optical spot size but rather by the spatial extent of the bias field (~10 nm).

The measured field $E_{emit}(t)$ should have its wavelength on the order of ~100 μm, which is 1 order of magnitude larger than the distance between two devices. This implies that it is the near-field component of $E_{emit}(t)$ that is measured in Figure 3D, which is confirmed by the polarization dependence experiment for the double-junction structure and the analysis based on the Hertzian dipole model[27] (see the Supporting Information).

By comparing the measurement for the case of $\Delta x = 12$ μm and $\Delta x = 6$ μm (see the Supporting Information), one sees that the finite time delay between the measurements for two devices can be tuned by the distance between them. This is a signature of the propagation of electric field from one device to the other.

This THz field can propagate from one junction to the other via three different media: vacuum, LAO, and STO. Both LAO and STO show strong dispersion and have much larger refractive index for THz frequencies.[28,29] Therefore, one expects the propagation time for $E_{emit}(t)$ in both oxide layers to be much longer than 40 fs. The dominant response is clearly coming from free-space propagation not strongly coupled to the LAO/STO interface. Much weaker dispersive effects are observed in both the single-junction and double-junction experiments; an investigation of the self-interaction of THz field within the LAO/STO system extends beyond the scope of this paper and will be discussed elsewhere.

As an oxide THz source and sensor, the LAO/STO nanojunctions offer several advantages compared to III−V semiconductor THz devices. The THz source/sensors described here are more than 1 order of magnitude smaller than devices described in the literature.[6,30] Semiconductor THz sources utilize real carrier absorption that limits the bandwidth of the generated THz fields to 1−2 THz;[6,30] by contrast, the spectral bandwidth of oxide nanojunctions appears to be limited only by the laser source (~10 THz for the experiments described here) due to the virtual resonance of the $\chi^{(3)}$ process. Finally, a single junction can act both as a source and detector to achieve the highest spatial and temporal resolution, which is

dx.doi.org/10.1021/nl401219v | Nano Lett. 2013, 13, 2884−2888

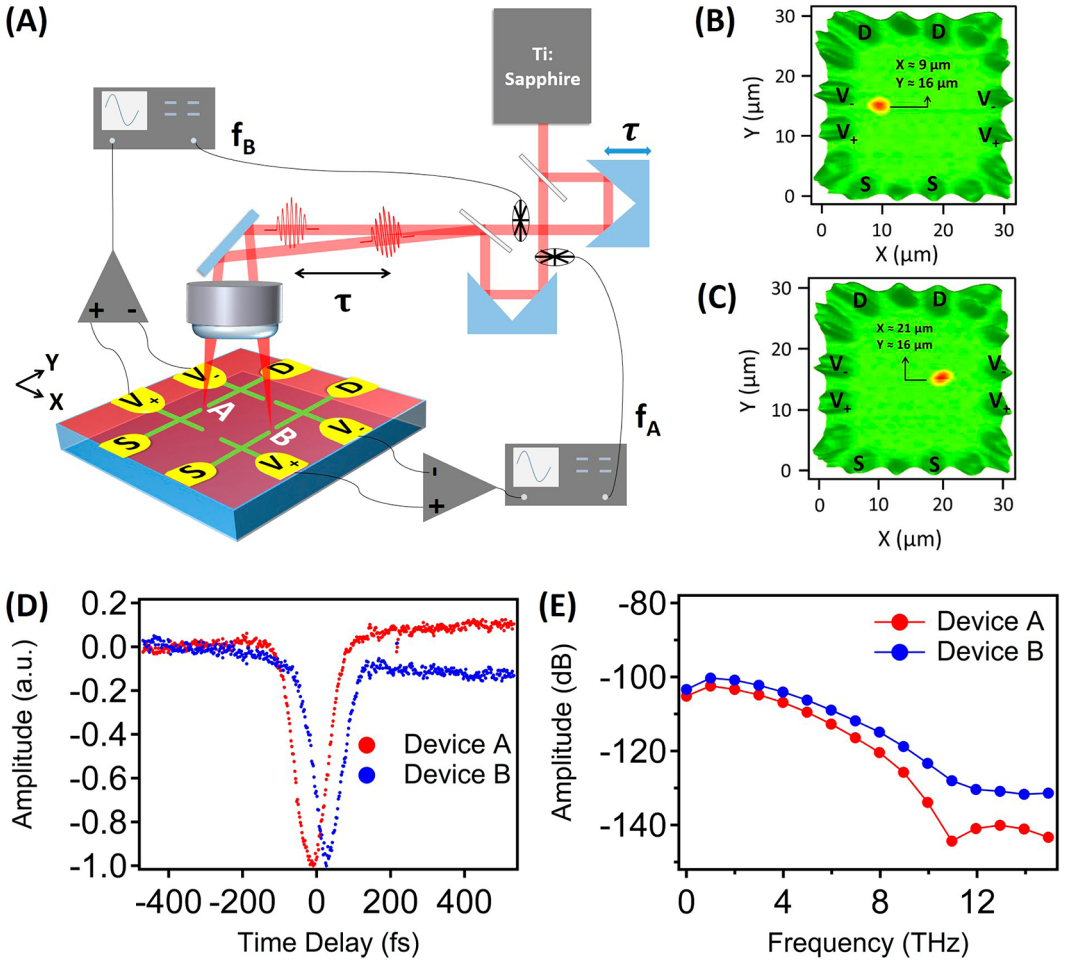

Figure 3. Two-junction measurement. (A) Experimental setup for double-junction measurement. The ODL is stepped, and no piezo shaker is used. (B,C) The image overlapped with the reflection image. Relevant electrodes are labeled to match (A). The coordinates are extracted from 2D Gaussian function fitting ($I_{ave} \approx 60$ KW/cm^2 and $V_s = -1$ V on both devices). (D) Time-resolved signal measured from the two devices. Each waveform is an average over 100 measurements ($I_{ave} \approx 70$ KW/cm^2 and $V_s = -1$ V for both devices). (E) FFT spectra of (D).

suitable for investigations of single molecules or other nanoscale objects.

One possible way to realize the imaging for a single molecule is to integrate a LAO/STO nanojunction-based THz emitter and detector platform with an atomic force microscope (AFM). The AFM can be exploited to locate the target of imaging. Afterward, the same AFM can be used to create both the emitter and detector in close proximity to the analyte, allowing the sensitivity to be greatly enhanced. Another approach involves electrostatic trapping of single particles at the junction.[31] By measuring the transport properties, one can determine whether the particle is trapped or not, and subsequently perform broadband THz spectroscopy[6] with and without the nanoparticle present. Motivated by the earlier work demonstrating the qubit manipulation with THz radiation,[8,32] once the target is located or trapped in our system, the nanoscale THz device enables the experiments of quantum operations in single molecules[33] or nanostructures.[34]

■ ASSOCIATED CONTENT

Supporting Information

Additional information and figures. This material is available free of charge via the Internet at http://pubs.acs.org.

■ AUTHOR INFORMATION

Corresponding Author

*E-mail: jlevy@pitt.edu.

Present Address

§Department of Electrical Engineering, Gachon University, Seongnam, South Korea, 461−701.

Author Contributions

The manuscript was written through contributions of all authors. All authors have given approval to the final version of the manuscript.

Notes

The authors declare no competing financial interest.

■ ACKNOWLEDGMENTS

The authors acknowledge support from AFOSR − FA9550-12-1-0268 (J.L.), AFOSR FA9550-12-1-0342 (C.-B.E.), and the National Science Foundation through Grants DMR-1104191 (J.L.) and DMR-1234096 (C.-B.E.).

■ REFERENCES

(1) Betzig, E.; Chichester, R. J. *Science* **1993**, *262* (5138), 1422−1425.
(2) Nie, S.; Emory, S. R. *Science* **1997**, *275*, 1102−1106.

(3) Zenhausern, F.; O'Boyle, M. P.; Wickramasinghe, H. K. *Appl. Phys. Lett.* **1994**, *65* (13), 1623−1625.
(4) Weiss, S. *Science* **1999**, *283*, 1676−1683.
(5) Guest, J. R.; Stievater, T. H.; Chen, G.; Tabak, E. A.; Orr, B. G.; Steel, D. G.; Gammon, D.; Katzer, D. S. *Science* **2001**, *293*, 2224−2227.
(6) Walther, M.; Fischer, B. M.; Ortner, A.; Bitzer, A.; Thoman, A.; Helm, H. *Anal. Bioanal. Chem* **2010**, *397*, 1009−1017.
(7) Huth, F.; Govyadinov, A.; Amarie, S.; Nuansing, W.; Keilmann, F.; Hillenbrand, R. *Nano Lett.* **2012**, *12*, 3973−3978.
(8) Cole, B. E.; Williams, J. B.; King, B. T.; Sherwin, M. S.; Stanley, C. R. *Nature* **2001**, *410*, 60−63.
(9) Huber, A. J.; Keilmann, F.; Wittborn, J.; Aizpurua, J.; Hillenbrand, R. *Nano Lett.* **2008**, *8*, 3766−3770.
(10) Knap, W.; Lusakowski, J.; Parenty, T.; Bollaert, S.; Cappy, A.; Popov, V. V.; Shur, M. S. *Appl. Phys. Lett.* **2004**, *84*, 2331−2333.
(11) Knap, W.; Deng, Y.; Rumyantsev, S.; Shur, M. S. *Appl. Phys. Lett.* **2002**, *81*, 4637−4639.
(12) Chen, H. T.; Kersting, R.; Cho, G. C. *Appl. Phys. Lett.* **2003**, *83*, 3009−3011.
(13) Kawano, Y. *IEEE J. Sel. Top. Quantum Electron.* **2011**, *17*, 67−78.
(14) Bitzer, A.; Ortner, A.; Walther, M. *Appl. Opt.* **2010**, *49*, E1−E6.
(15) Ohtomo, A.; Hwang, H. Y. *Nature* **2004**, *427*, 423−426.
(16) Cen, C.; Thiel, S.; Hammerl, G.; Schneider, C. W.; Andersen, K. E.; Hellberg, C. S.; Mannhart, J.; Levy, J. *Nat. Mater.* **2008**, *7*, 298−302.
(17) Cen, C.; Thiel, S.; Mannhart, J.; Levy, J. *Science* **2009**, *323*, 1026.
(18) Bogorin, D. F.; Bark, C. W.; Jang, H. W.; Cen, C.; Folkman, C. M.; Eom, C. B.; Levy, J. *Appl. Phys. Lett.* **2010**, *97*, 013102.
(19) Cheng, G.; Siles, P. F.; Bi, F.; Cen, C.; Bogorin, D. F.; Bark, C. W.; Folkman, C. M.; Park, J. W.; Eom, C. B.; Ribeiro, G. M.; Levy, J. *Nat. Nanotechnol.* **2011**, *6*, 343−347.
(20) Irvin, P.; Ma, Y.; Bogorin, D. F.; Cen, C.; Bark, C. W.; Folkman, C. M.; Eom, C. B.; Levy, J. *Nat. Photonics* **2010**, *4*, 849−852.
(21) Nakamura, R.; Kanematsu, Y. *Rev. Sci. Instrum.* **2004**, *75*, 636−644.
(22) Basletic, M.; Maurice, J.-L.; Carrétéro, C.; Herranz, G.; Copie, O.; Bibes, M.; Jacquet, É.; Bouzehouane, K.; Fusil, S.; Barthélémy, A. *Nat. Mater.* **2008**, *7*, 621−625.
(23) Hu, B. B.; Zhang, X. C.; Auston, D. H. *Phys. Rev. Lett.* **1991**, *67* (19), 2709.
(24) Chen, J.; Han, P.; Zhang, X.-C. *Appl. Phys. Lett.* **2009**, *95*, 011118.
(25) Ahn, Y.; Dunning, J.; Park, J. *Nano Lett.* **2005**, *5*, 1367−1370.
(26) Kawano, Y.; Ishibashi, K. *Nat. Photonics.* **2008**, *2*, 618−621.
(27) Auston, D. H.; Cheung, K. P.; Smith, P. R. *Appl. Phys. Lett.* **1984**, *45*, 284.
(28) Grischkowsky, D.; Keiding, S. *Appl. Phys. Lett.* **1990**, *57*, 1055−1057.
(29) Han, J.; Wan, F.; Zhu, Z.; Zhang, W. *Appl. Phys. Lett.* **2007**, *90*, 031104.
(30) Shan, J.; Heinz, T. F. *Top. Appl. Phys.* **2004**, *92*, 1−59.
(31) Bezryadin, A.; Dekker, C.; Schmid, G. *Appl. Phys. Lett.* **1997**, *71*, 1273−1275.
(32) Santambrogio, G.; Meek, S. A.; Abel, M. J.; Duffy, L. M.; Meijer, G. *ChemPhysChem* **2011**, *12* (10), 1799−1807.
(33) DeMille, D. *Phys. Rev. Lett.* **2002**, *88* (6), 067901.
(34) Levy, J. *Phys. Rev. A* **2001**, *64*, 052306.